Black Sea Journal of Engineering and Science
doi: 10.34248/bsengineering.1733519

Open Access Journal
e-ISSN: 2619 – 8991

Research Article
Volume 8 - Issue 5: 1577-1584 / September 2025

ENHANCED PHOTOCATALYTIC DEGRADATION OF METHYL RED DYE VIA HYDROTHERMALLY SYNTHESIZED MANGANESE TUNGSTATE

Mehmet KAYHAN[1]*

[1]*Usak University, Usak University Scientific Analysis, Technological Application and Research Center, 64000, Uşak, Türkiye*

Abstract: In this study, $MnWO_4$ nanoparticles were successfully synthesized via a CTAB-assisted hydrothermal method and evaluated for their photocatalytic degradation performance against Methyl Red (MR) dye under UV-C irradiation. Structural and morphological characterizations were performed using XRD, FTIR, SEM, and UV-DRS techniques, confirming the formation of highly crystalline monoclinic $MnWO_4$ with defect-rich surfaces. The photocatalytic experiments were conducted under UV-C light (254 nm) with a catalyst dosage of 0.5 g/L, initial MR concentration of 20 mg/L, and solution pH of 6.5. The synthesized $MnWO_4$ exhibited excellent degradation efficiency, achieving 98% MR removal within 90 minutes, outperforming several conventional photocatalysts. This work addresses a critical gap in the literature by demonstrating the enhanced activity of CTAB-modified $MnWO_4$ under UV-C light, offering a promising route for azo dye remediation. The findings suggest that morphology control and surface defect engineering significantly influence photocatalytic performance, making $MnWO_4$ a viable candidate for environmental applications.

Keywords: Manganese tungstate, Hydrothermal synthesis, Methyl red, UV-C photocatalysis, Azo dye degradation, Band gap engineering

***Corresponding author:** Usak University, Usak University Scientific Analysis, Technological Application and Research Center, 64000, Uşak, Türkiye
E mail: mehmet.kayhan@usak.edu.tr (M. KAYHAN)
Mehmet KAYHAN https://orcid.org/0000-0002-4581-2657

Received: July 03, 2025
Accepted: September 08, 2025
Published: September 15, 2025

Cite as: Kayhan M. 2025. Enhanced photocatalytic degradation of methyl red dye via hydrothermally synthesized manganese tungstate. BSJ Eng Sci, 8(5): 1577-1584.

1. Introduction

Industrial dyes, particularly azo dyes such as Methyl Red (MR), pose serious threats to aquatic ecosystems and human health due to their toxic, carcinogenic, and non-biodegradable nature (Ahmad et al., 2015; Ahmad et al., 2019; Alharbi et al., 2024). The uncontrolled discharge of dye-laden effluents from industries such as textiles, leather processing, and printing significantly contributes to water pollution, adversely affecting photosynthetic activity and ecological balance (He et al., 2010; Berradi et al., 2019; Allabakshi et al., 2025). The visible coloration of even trace amounts in water can inhibit photosynthesis by obstructing light penetration, leading to ecological imbalances (He et al., 2010). Conventional wastewater treatment methods, including coagulation, adsorption, and biological degradation, often fail to adequately remove such persistent organic contaminants (Shivaganga et al., 2023; Shamshad and Ur Rehman, 2025). So, the rapid release of these dyes into water necessitates the development of effective and sustainable wastewater treatment technologies.

To address these concerns advanced oxidation processes (AOPs), particularly semiconductor-based photocatalysis, has emerged as a green, sustainable, and cost-effective approach for degrading organic dyes under light irradiation among alternative methods (Kayhan et al., 2024; Shalini et al., 2024; Nagaraja et al., 2025; Nezzari et al., 2025; Rastin et al., 2025). This method utilizes semiconductor materials that generate reactive oxygen species (ROS), leading to the breakdown of complex dye molecules into harmless byproducts such as CO_2 and H_2O (Kumar et al., 2021; Jayakumar et al., 2024). The success of photocatalysis depends significantly on the optical and structural properties of the catalyst used.

In this context, among various semiconductors, transition metal tungstates (Kayhan, 2025a; Kayhan, 2025b), and particularly manganese tungstate ($MnWO_4$), have drawn increasing attention due to their favorable optical and electronic properties. $MnWO_4$, a monoclinic wolframite-type oxide, possesses a favorable bandgap energy (~1.75–2.8 eV) that facilitates visible-light-driven photocatalytic reactions (He et al., 2010; Kumar et al., 2021; Jayakumar et al., 2024). In addition to its stability and cost-effectiveness, $MnWO_4$ exhibits unique physicochemical properties, including high photostability, versatile electronic properties, magnetic behavior and multiferroicity, which further enhance its versatility for environmental (Khaksar et al., 2015; Kumar et al., 2021). These properties make $MnWO_4$ an attractive candidate not only in photocatalysis but also in electrocatalysis, gas

sensing, and energy storage systems (Khaksar et al., 2015; Vosoughifar, 2017).

Previous studies have demonstrated the effectiveness of $MnWO_4$ in degrading organic dyes such as methyl orange and methylene blue under UV and visible light sources (Vosoughifar, 2017; Shivaganga et al., 2023; Kayhan and Kayhan, in press). The photocatalytic performance of $MnWO_4$ is greatly influenced by factors such as synthesis parameters such as pH, temperature, and precursor concentration, particle morphology and surface area (Wu et al., 2012; Jayakumar et al., 2024). For instance, $MnWO_4$ exhibits nanorod or needle-like morphologies that promote efficient charge separation, enhancing photocatalytic performance (Vosoughifar, 2017; Kayhan Kayhan, in press).

Several studies have explored $MnWO_4$-based composite materials to enhance photocatalytic performance by facilitating charge separation and extending light absorption range. For example, $MnWO_4$–TiO_2 nanoflower composites have demonstrated superior degradation efficiency of methyl orange under visible light, attributed to the formation of heterojunctions that promote effective electron-hole separation (Hassan et al., 2015). Additionally, incorporation of conductive materials like reduced graphene oxide (RGO) has shown to enhance surface area and charge carrier mobility, further improving photocatalytic activity (Siahsahlan et al., 2025). Despite this growing body of research and promising results in the degradation of dyes like methylene blue and methyl orange, research specifically focused on the visible-light-driven degradation of Methyl Red using the standalone performance of hydrothermally synthesized pure $MnWO_4$ remains underexplored. Therefore, given MR's recalcitrant nature and environmental significance, this study aims to synthesize $MnWO_4$ nanoparticles via a controlled hydrothermal method, characterize their structural and optical properties, and evaluate their photocatalytic performance against MR dye under UV-light.

2. Materials and Methods

2.1. Materials

The chemicals used in the synthesis such as Sodium tungstate dihydrate ($Na_2WO_4.2H_2O$, 99+% ACS Reagent purity from Thermo Scientific) and Manganese chloride tetrahydrate ($MnCl_2.4H_2O$, analytical grade from Thermo Scientific), Hexadecyltrimethylammonium bromide (CTAB, 99+% purity from Thermo Scientific), methyl red were ACS reagent grade purchased from Supelco and they were used without any purification.

2.2. Synthesis of Manganese Tungstate

To initiate the synthesis, 2.0 g of sodium tungstate dihydrate ($Na_2WO_4{\cdot}2H_2O$) was accurately weighed and dissolved in distilled water to obtain 100 mL of stock solution using a volumetric flask. A 10 mL aliquot of this solution was then transferred into a 100 mL glass beaker and diluted with an additional 40 mL of distilled water. Subsequently, 150 mg of cetyltrimethylammonium bromide (CTAB) was added as a surfactant to assist in controlling particle growth and morphology.

The resulting mixture was stirred magnetically for 5 minutes to ensure complete dissolution of the CTAB. Thereafter, 485 mg of manganese(II) chloride tetrahydrate ($MnCl_2{\cdot}4H_2O$) was gradually introduced into the solution under continuous stirring. The reaction mixture was further stirred for 40 minutes to allow for homogeneous mixing and precursor interaction.

Following the mixing step, the solution was transferred into a Teflon-lined stainless steel autoclave and subjected to hydrothermal treatment at 140 °C for 24 hours. Upon completion of the reaction, the resulting precipitates were collected by vacuum filtration, thoroughly rinsed with distilled water to remove residual ions and surfactant, and subsequently dried at ambient temperature overnight.

2.3. Characterization

The crystalline structure and phase composition of the hydrothermally synthesized $MnWO_4$ samples were analyzed using X-ray diffraction (XRD) with Cu Kα radiation, scanned over a 2θ range of 10° to 65° (Rigaku Miniflex X-Ray Diffractometer). Functional groups and chemical bonding characteristics were examined via Fourier-transform infrared (FTIR) spectroscopy in the range of 400–4000 cm^{-1} using an ATR-equipped spectrometer (Spectrum Two, Perkin Elmer). Optical properties and band gap estimation were obtained through UV–Visible Diffuse Reflectance Spectrophotometer (UV-DRS) within the 300–800 nm wavelength range (SHIMADZU 2600i). The surface morphology and microstructural features of the materials were observed using a scanning electron microscope (SEM) equipped with a CeB_6 electron source (Phenom ProX SEM).

2.4. Photocatalytic Behavior Evaluation of Manganese Tungstate

Photocatalytic performance was evaluated using a custom-fabricated reactor system consisting of a cylindrical quartz vessel surrounded by six symmetrically arranged 8 watt UV-C lamps positioned at a distance of 25 mm from the quartz reactor. The configuration was designed to ensure uniform irradiation of the reaction medium. Throughout the experiments, the solution inside the reactor was continuously stirred with a magnetic stirrer, while a steady flow of air was bubbled into the system to maintain both oxygenation and solution homogeneity at 25±2°C. To mitigate any thermal effects induced by prolonged UV exposure, the reactor's outer chamber was cooled by ambient air circulation.

The model pollutant, Methyl Red (MR), was initially prepared as a 400 mg/L stock solution in a solvent mixture of ethanol and distilled water (40:60, v/v). This stock solution was then diluted with distilled water to obtain a 10 mg/L working solution in a total volume of 500 mL. The pH of the solution was adjusted to 1.5 using hydrochloric acid (HCl) to simulate acidic conditions favorable for MR degradation.

For each experiment, 200 mg of the synthesized

manganese tungstate catalyst was added to the dye solution. Prior to irradiation, the suspension was stirred and aerated for 30 minutes in the dark to establish adsorption–desorption equilibrium between the catalyst surface and the dye molecules.

Photocatalytic degradation of MR was monitored using a UV-Visible spectrophotometer (PerkinElmer Lambda 35). An initial absorbance spectrum was recorded at 0 minutes following the adsorption phase. Thereafter, the reactor was exposed to UV-C illumination, and absorbance measurements were taken at 15-minute intervals for a total irradiation duration of 180 minutes. Spectral data were collected in the 300–650 nm wavelength range to track the progressive decomposition of MR over time.

3. Results and Discussion

The manganese tungstate photocatalyst was successfully synthesized via a hydrothermal method. In order to comprehensively investigate its structural properties, XRD analysis was performed.

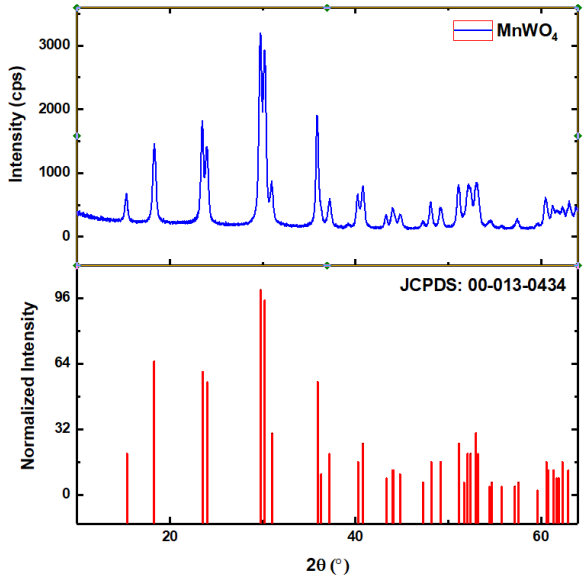

Figure 1. XRD pattern of $MnWO_4$.

The crystallographic structure of the hydrothermally synthesized manganese tungstate ($MnWO_4$) was confirmed by X-ray diffraction (XRD) analysis (Figure 1). The diffraction peaks observed in the XRD pattern correspond precisely to those of monoclinic phase with a wolframite-type crystal structure of $MnWO_4$ and are in excellent agreement with the standard data from the Joint Committee on Powder Diffraction Standards (JCPDS Card No. 00-013-0434). No secondary or impurity phases were detected, indicating the high phase purity of the product. The sharp and well-defined diffraction peaks suggest the formation of a well-crystallized structure. This result confirms that the hydrothermal method employed in this study is effective in producing phase-pure $MnWO_4$ with the desired crystalline characteristics. The absence of extraneous peaks also implies that no residual precursors or unintended by-products are present in the final material.

Figure 2 presents SEM micrographs of hydrothermally synthesized $MnWO_4$ particles prepared in the presence of CTAB surfactant, recorded at magnifications of 10,000× (Figure 2A) and 30,000× (Figure 2B). The images clearly reveal that the $MnWO_4$ particles exhibit predominantly spherical to sub-spherical morphologies with a relatively uniform size distribution. Unlike the needle-like structures typically observed in $MnWO_4$ synthesized via coprecipitation routes (Kayhan and Kayhan, in press), the use of CTAB during hydrothermal synthesis appears to suppress anisotropic growth, promoting more isotropic and equiaxed particle formation.

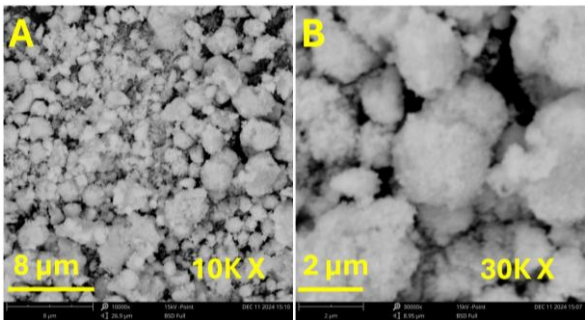

Figure 2. SEM images of hydrothermally synthesized $MnWO_4$.

This suggests that the synthesis conditions—particularly the presence of surfactants—play a crucial role in directing the formation of highly controlled and uniform nanoparticles, rather than the aggregated structures commonly associated with hydrothermal processes (Wang et al., 2020). The observed morphological transition can be attributed to the surface-active nature of CTAB, which likely adsorbs preferentially on specific crystal facets, thereby modulating the relative growth rates and favoring spherical particle assembly (Rao and Cölfen, 2017). Mild particle agglomeration is also observed, which is typical for hydrothermally derived oxides due to Van der Waals interactions during the drying stage (Grass et al., 2006). Nevertheless, the overall microstructure indicates good homogeneity and potential for enhanced surface reactivity. The selective adsorption of CTAB facilitates fine-tuning of particle morphology by controlling surface energies, enabling the formation of structures not typically achievable through conventional growth mechanisms (Maya-Johnson et al., 2017).

The morphological findings are in strong agreement with the XRD results, which confirmed the formation of monoclinic $MnWO_4$ with high crystallinity and no detectable secondary phases. The absence of sharp anisotropic features in the SEM images is consistent with the broadened but symmetrical diffraction peaks in the XRD patterns, suggesting that the particles are nanocrystalline and structurally uniform across different orientations.

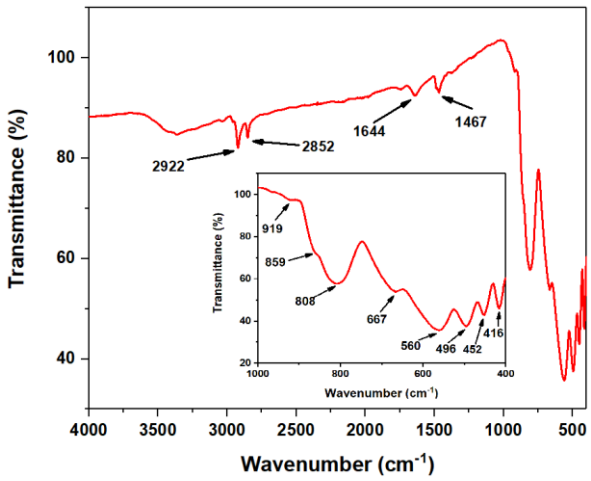

Figure 3. FTIR spectrum of $MnWO_4$. Inset shows the bands in the range of 1000-400cm-1.

The FTIR spectrum of hydrothermally synthesized $MnWO_4$ is presented in Figure 3, with an inset highlighting the fingerprint region between 1000 and 400 cm^{-1}. The observed spectral bands confirm the formation of $MnWO_4$ and the successful incorporation of CTAB as a structure-directing agent during synthesis. Characteristic CH_2 stretching vibrations of the amine group were identified at 2922 cm^{-1} (asymmetric) and 2852 cm^{-1} (symmetric), accompanied by a CH_3 bending vibration at 1467 cm^{-1}, N–H bending (from CTAB) at 1644 cm^{-1} which are in agreement with previous reports on CTAB-assisted metal tungstates (Xue et al., 2007; Kayhan M, 2025). These features indicate the possible presence of residual CTAB molecules or their interaction with the oxide surface.

In the lower wavenumber region, several distinct peaks were observed between 1000 and 400 cm^{-1}. The sharp band at 919 cm^{-1} is assigned to the stretching vibration of terminal W=O bonds, while the bands at 859 cm^{-1} and 808 cm^{-1} correspond to the symmetric and asymmetric stretching modes of W–O bonds in the WO_4 tetrahedra (Pirhashemi et al., 2018; Kayhan and Kayhan, in press). A band at 667 cm^{-1} is associated with the asymmetric stretching of W–O bonds in the $(W_2O_4)_n$ structural network. Additional peaks at 560 cm^{-1} and 496 cm^{-1} are attributed to Mn–O stretching vibrations, confirming the integration of manganese into the oxide framework (Zheng et al., 2013; Muthamizh et al., 2015). A weak peak at 452 cm^{-1} is linked to the in-plane deformation of the longest W–O bond, while the band at 416 cm^{-1} is assigned to the bending mode of W–O in the WO_2 terminals (Muthamizh et al., 2015).

Moreover, CTAB-assisted $MnWO_4$ exhibited minor shifts in the Mn–O stretching region, which may be indicative of subtle structural perturbations. These shifts could possibly reflect weak substitutional effects or partial coordination involving bromine species, such as Mn–Br, as suggested in similar CTAB-mediated tungstate systems (Luo et al., 2018; Zargazi and Entezari, 2019). This could possibly suggest the formation of disordered $[WO_{6-x}Br_{2x}]$ species due to the presence of bromide ions, which disturb the local coordination geometry of tungsten. Such distortion may facilitate the creation of electron traps or oxygen vacancies, forming active surface sites that contribute to enhanced properties in photocatalytic or photochromic responses (Kayhan E, 2025; Kayhan M, 2025).

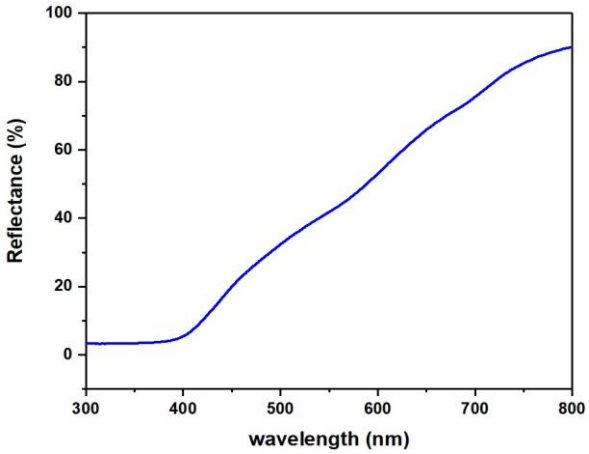

Figure 4. Reflectance data of MnWO4 via UV-DRS.

The optical properties of the synthesized $MnWO_4$ sample were investigated using UV–visible diffuse reflectance spectroscopy (UV-DRS), as shown in Figure 4. A sharp absorption edge exhibits near 395 nm, indicative of a band gap characteristic of tungstate-based semiconductors. The reflectance gradually increases with wavelength, reaching approximately 90% at 800 nm. A weak reflectance shoulder peak was detected at approximately 512 nm, which is attributed to the electronic transition from O-2p to Mn-3d states within the $MnWO_4$ structure. In addition to this, a weaker yet distinct absorption band was observed near 640 nm, which is assigned to the spin-forbidden electronic transition between the e_g and t_{2g} orbitals of the Mn-3d states (Nogami et al., 2008). These transitions are characteristic of Mn^{2+} ions in a distorted octahedral coordination, as expected for wolframite-type $MnWO_4$, and are in good agreement with the XRD results confirming the formation of a single-phase monoclinic structure with high crystallinity.

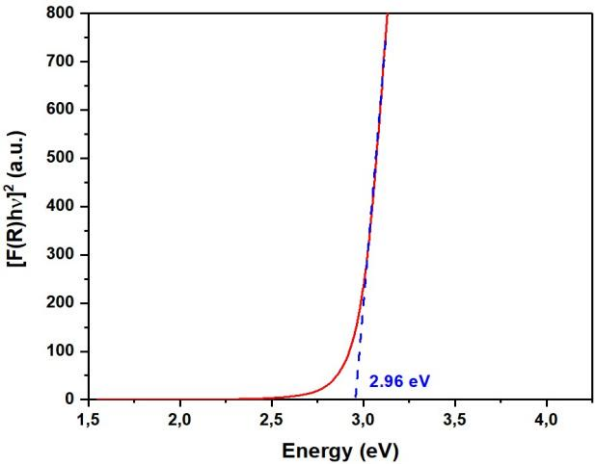

Figure 5. Direct band gap of $MnWO_4$.

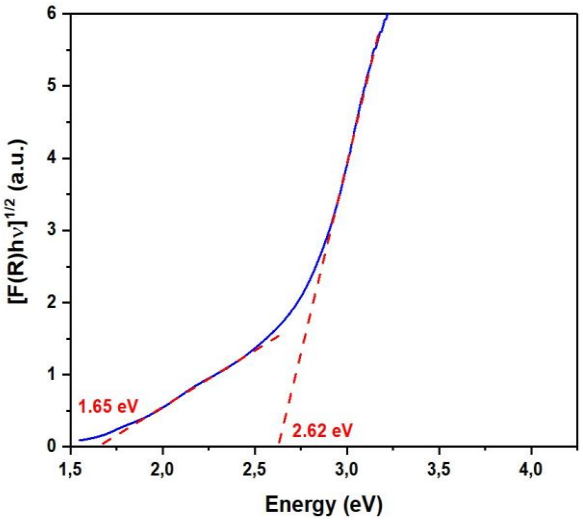

Figure 6. Indirect band gap of $MnWO_4$.

The optical band gap (E_g) of the synthesized $MnWO_4$ nanostructures was estimated using the Tauc method, based on the Kubelka–Munk transformation of diffuse reflectance data. The Tauc plot was constructed by plotting $[F(R)h\nu]^n$ versus photon energy ($h\nu$), where F(R) denotes the Kubelka–Munk function, h is Planck's constant, and ν is the frequency of the incident light. The value of the exponent *n* in the Tauc relation depends on the nature of the electronic transition, with $n = ½$ for indirect allowed transitions and $n = 2$ for direct allowed transitions. The optical band gap was determined by extrapolating the linear region of the plot to the energy axis, where$[F(R)h\nu]^n = 0$.

In the present study, the Tauc plots revealed both an indirect and a direct band gap for $MnWO_4$, consistent with the semiconducting nature of tungstate-based oxides. The indirect band gap was found to be approximately 1.65 eV and 2.62 eV (Figure 6), whereas the direct band gap was estimated to be around 2.96 eV (Figure 5). These values align well with previously reported band gaps of $MnWO_4$ nanostructures synthesized via hydrothermal and microwave-assisted routes (Almeida et al., 2012; Chakraborty et al., 2012). The presence of both direct and indirect transitions suggests that the optical behavior of $MnWO_4$ may be influenced by its microstructure, crystallite size, or surface states induced during synthesis, particularly in the presence of surfactants like CTAB.

Compared to our earlier work in which $MnWO_4$ was synthesized via a conventional solid-state route (Kayhan and Kayhan, in press), the hydrothermal method used in this study yielded lower band gap values. In the previous study, indirect band gaps were determined as 1.72 eV and 2.76 eV, while the direct band gap was measured at 3.18 eV. This downward shift in energy levels is indicative of enhanced light absorption in the visible range. Such narrowing of the band gap may arise not only from morphological and crystallinity differences, but also from structural disorder introduced during synthesis, as evidenced by FTIR analysis. Specifically, the CTAB-assisted $MnWO_4$ exhibited subtle shifts in the Mn–O stretching region and signatures of bromine-influenced $[WO_{6-x}Br_{2x}]$ species. These features suggest that bromide ions may have partially substituted oxygen within the coordination sphere of tungsten, thereby inducing local distortions and creating electron traps or oxygen vacancies (Luo et al., 2018; Zargazi and Entezari, 2019). Such defect-related states are known to facilitate charge carrier separation and enhance the generation of reactive species under illumination.

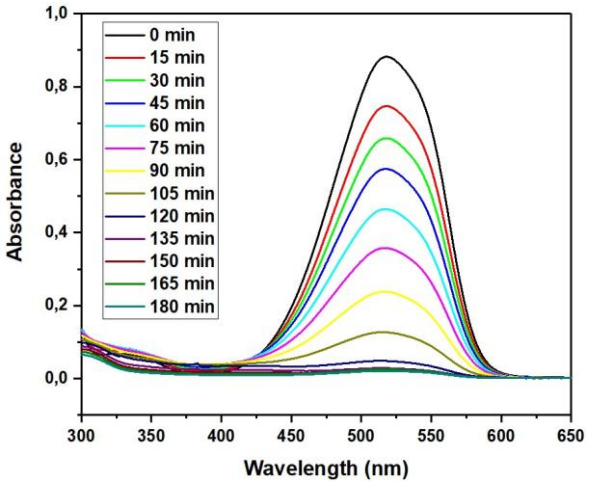

Figure 7. UV–Vis spectra of methyl red solution during photocatalytic degradation by $MnWO_4$ over 180 minutes.

Figure 7 shows the change in absorbance of methyl red using hydrothermally synthesized MnWO4 as a photocatalyst over time at every 15 minutes within the time interval of 0–180 minutes.

The initial spectrum (black line at 0 min) shows a strong absorbance peak around 518 nm is associated with the azo chromophore (–N=N–) group of methyl red, corresponding to the characteristic absorption of methyl red (MR) in aqueous solution. As time elapses, the intensity of this peak decreases steadily, indicating the progressive breakdown of the MR dye molecules. The degradation efficiency increases rapidly during the first 120 minutes, reaching over 90%. Between 135–180 minutes, the curve plateaus near 95–97%, suggesting a saturation point or equilibrium. The near-complete degradation (close to 100%) highlights the high photocatalytic activity of $MnWO_4$. After 180 minutes, the absorbance at 518 nm is nearly zero, suggesting almost complete degradation of methyl red.

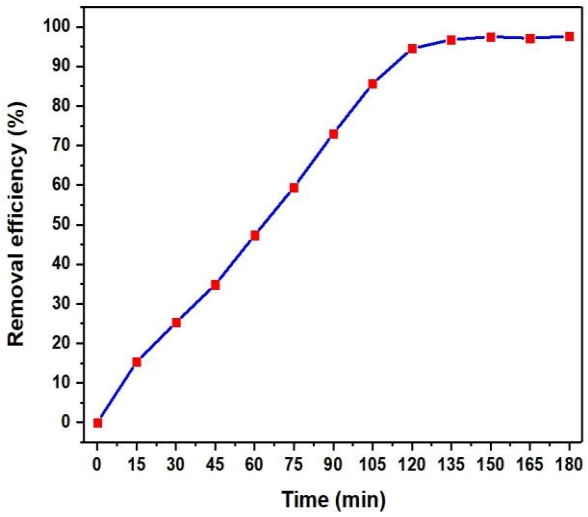

Figure 8. Removal efficiency of MnWO4 on the photodegradation of Methyl Red dye.

The improvement in optical properties directly translated into superior photocatalytic activity. While the solid-state-derived $MnWO_4$ achieved only ~60% degradation of methylene blue after 180 minutes, the hydrothermally synthesized counterpart reached 98% under identical conditions (Figure 8). These findings highlight the synergistic effect of controlled synthesis, defect engineering, and surfactant-assisted structural modulation on the functional performance of $MnWO_4$-based photocatalysts. The near-complete degradation (close to 100%) highlights the high photocatalytic activity of $MnWO_4$.

The superior photocatalytic performance of $MnWO_4$ synthesized via the CTAB-assisted hydrothermal method can be attributed to its controlled morphology and defect-rich surfaces, which enhance charge separation and light absorption. Compared to conventional photocatalysts such as TiO_2 and ZnO under different light sources, the $MnWO_4$ system demonstrated significantly higher degradation efficiency under UV-C irradiation. For instance, TiO_2 achieved 85% methyl red removal in 120 minutes under UV-A light (Zhang et al., 2021), while ZnO reached only 54% removal under sunlight in 180 minutes (Gaim et al., 2019). Recent studies on g-C_3N_4 and its composites have also explored azo dye degradation under sunlight, reporting efficiencies of 97% for pristine g-C_3N_4 in 120 minutes (Sahoo et al., 2024) and 95% for g-C_3N_4/$MnWO_4$ heterojunctions in 120 minutes (Li et al., 2025). Similarly, $MnWO_4$-based composites such as $MnWO_4$/WO_3 have shown 88% methyl orange removal in 120 minutes under sunlight (Jayakumar et al., 2024). Moreover, $MnWO_4$ ceramic nanomaterials demonstrated excellent performance, achieving 98% methylene blue degradation under visible light in 120 minutes (Shivaganga et al., 2023). Although these systems demonstrate good sunlight activity, their performance strongly depends on solar irradiation and longer treatment times. While previous $MnWO_4$-based systems have shown promising results, they generally reported lower efficiencies under UV-C. For example, a closely related study reported only 60% methyl red removal after 180 minutes without CTAB modification (Kayhan and Kayhan, in press). In contrast, the current $MnWO_4$ system achieved 98% degradation within 90 minutes under UV-C, highlighting its potential as a more effective alternative. Thus, this work clearly differentiates itself by demonstrating enhanced performance through surfactant-assisted synthesis, validating the role of CTAB in improving photocatalytic activity. These comparative results are summarized in Table 1, highlighting the superior performance of CTAB-assisted $MnWO_4$ relative to conventional and previously reported photocatalysts.

Table 1. Comparative photocatalytic performance of $MnWO_4$ and benchmark catalysts (TiO_2, ZnO, g-C_3N_4, Bi_2WO_6) for azo dye degradation under various light sources. The enhanced efficiency of CTAB-assisted $MnWO_4$ under UV-C irradiation is highlighted relative to previously reported systems

Photocatalyst	Light Source	Dye Type	Degradation Efficiency (%)	Time (min)	Reference
TiO_2	UV-A	Methyl Red	85	120	(Zhang et al. 2021)
ZnO	Sunlight	Methyl Red	54	180	(Gaim et al. 2019)
g-C_3N_4	Sunlight	Methyl Red	97	120	(Sahoo et al. 2024)
g-C_3N_4/$MnWO_4$ heterojunction	Sunlight	Azo dyes (CR, MB)	95	120	(Li et al. 2025)
$MnWO_4$/WO_3 nanocomposite	Sunlight	Methyl Orange	88	120	(Jayakumar et al. 2024)
$MnWO_4$ ceramic nanomaterial	Visible	Methylene Blue	98	120	(Shivaganga et al. 2023)
$MnWO_4$	UV-C	Methyl Red	60	180	(Kayhan and Kayhan, in press)
$MnWO_4$	UV-C	Methyl Red	98	90	This study

5. Conclusion

In conclusion, $MnWO_4$ nanoparticles synthesized via CTAB-assisted hydrothermal method demonstrated remarkable photocatalytic efficiency, achieving 98% degradation of Methyl Red dye under UV-C irradiation. This high performance is attributed to the controlled morphology and defect-rich surfaces, which enhance light absorption and charge separation. The structural features confirmed by XRD, SEM, FTIR, and UV-DRS analyses directly correlate with the observed photocatalytic activity. These findings highlight the potential of $MnWO_4$ as a cost-effective and efficient photocatalyst for azo dye remediation. Given its strong degradation capability and reproducible synthesis, $MnWO_4$ may be considered for future environmental applications, particularly in wastewater treatment technologies.

Author Contributions

The percentages of the author' contributions are presented below. The author reviewed and approved the final version of the manuscript.

	M.K.
C	100
D	100
S	100
DCP	100
DAI	100
L	100
W	100
CR	100
SR	100
PM	100
FA	100

C=Concept, D= design, S= supervision, DCP= data collection and/or processing, DAI= data analysis and/or interpretation, L= literature search, W= writing, CR= critical review, SR= submission and revision, PM= project management, FA= funding acquisition.

Conflict of Interest

The author declared that there is no conflict of interest.

Ethical Consideration

Ethics committee approval was not required for this study because of there was no study on animals or humans.

References

Ahmad MA, Ahmad N, Bello OS. 2015. Modified durian seed as adsorbent for the removal of methyl red dye from aqueous solutions. Appl Water Sci, 5(4): 407–423. https://doi.org/10.1007/s13201-014-0208-4

Ahmad MA, Ahmed NB, Adegoke KA, Bello OS. 2019. Sorption studies of methyl red dye removal using lemon grass (Cymbopogon citratus). Chem Data Collect, 22: 100249. https://doi.org/10.1016/j.cdc.2019.100249

Alharbi AA, Aldaghri O, El-Badry BA, Ibnaouf KH, Alfadhl F, Albadri A, Modwi A. 2024. Degradation of methyl red dye via fabricated Y_2O_3–MgO/g-C_3N_4 nanostructures: modification of band gap and photocatalysis under visible light. Opt Mater, 152: 115443. https://doi.org/10.1016/j.optmat.2024.115443

Allabakshi SM, Srikar PSNSR, Gangwar RK, Maliyekkal SM. 2025. Nonthermal plasma technology for degradation of dyes in wastewater. In: Hamdaoui O (Ed.), Innovative and Hybrid Advanced Oxidation Processes for Water Treatment. Elsevier, pp: 255–278. https://doi.org/10.1016/B978-0-443-14100-3.00001-6

Almeida MAP, Cavalcante LS, Varela JA, Li MS, Longo E. 2012. Effect of different surfactants on the shape, growth and photoluminescence behavior of $MnWO_4$ crystals synthesized by the microwave-hydrothermal method. Adv Powder Technol, 23(1): 124–128. https://doi.org/10.1016/j.apt.2011.10.004

Berradi M, Hsissou R, Khudhair M, Assouag M, Cherkaoui O, El Bachiri A, El Harfi A. 2019. Textile finishing dyes and their impact on aquatic environs. Heliyon, 5(11): e02711. https://doi.org/10.1016/j.heliyon.2019.e02711

Chakraborty AK, Ganguli S, Kebede MA. 2012. Photocatalytic degradation of 2-propanol and phenol using Au loaded $MnWO_4$ nanorod under visible light irradiation. J Cluster Sci, 23(2): 437–448. https://doi.org/10.1007/s10876-012-0450-6

Gaim YT, Tesfamariam GM, Nigussie GY, Ashebir ME. 2019. Synthesis, characterization and photocatalytic activity of N-doped Cu_2O/ZnO nanocomposite on degradation of methyl red. J Compos Sci, 3(4): 93. https://doi.org/10.3390/jcs3040093

Grass RN, Tsantilis S, Pratsinis SE. 2006. Design of high-temperature, gas-phase synthesis of hard or soft TiO_2 agglomerates. AIChE J, 52(4): 1318–1325. https://doi.org/10.1002/aic.10739

Hassan MS, Amna T, Al-Deyab SS, Kim HC, Khil MS. 2015. Monodispersed 3D $MnWO_4$–TiO_2 composite nanoflowers photocatalysts for environmental remediation. Curr Appl Phys, 15(6): 753–758. https://doi.org/10.1016/j.cap.2015.03.022

He HY, Huang JF, Cao LY, Wu JP. 2010. Photodegradation of methyl orange aqueous on $MnWO_4$ powder under different light resources and initial pH. Desalination, 252(1): 66–70. https://doi.org/10.1016/j.desal.2009.10.024

Jayakumar P, Palani S, Nallathambi M, Kuppusamy K. 2024. Evaluation of $MnWO_4$ nanomaterial for enhanced photocatalytic degradation activity over methyl orange. Lett Appl NanoBioSci, 13(1): 1. https://doi.org/10.33263/lianbs131.001

Kayhan E. 2025a. Temperature-controlled synthesis of bismuth tungstate with enhanced photochromic properties. Int J Appl Ceram Technol, 22(3): e15079. https://doi.org/10.1111/ijac.15079

Kayhan M, Aksoy M, Kayhan E. 2024. A facile synthesis of photocatalytic $Fe(OH)_3$ nanoparticles for degradation of phenol. ChemistrySelect, 9(23): e202401367. https://doi.org/10.1002/slct.202401367

Kayhan M. 2025b. Comparative study of photochromic behavior of bismuth tungstate via different surfactants. Ceram Int, 51(14): 19579–19588. https://doi.org/10.1016/j.ceramint.2025.02.133

Khaksar M, Boghaei DM, Amini M. 2015. Synthesis, structural characterization and reactivity of manganese tungstate nanoparticles in the oxidative degradation of methylene blue. C R Chim, 18(2): 199–203. https://doi.org/10.1016/j.crci.2014.04.004

Kumar KS, Vaishnavi K, Venkataswamy P, Ravi G, Ramaswamy K, Vithal M. 2021. Photocatalytic degradation of methylene blue over N-doped $MnWO_4$ under visible light irradiation. J Indian Chem Soc, 98(10): 100140. https://doi.org/10.1016/j.jics.2021.100140

Li R, Du Y, Tang C, Huang Y, Han G. 2025. Photocatalytic degradation of azo dye wastewater by thermal stripping of g-C_3N_4. In: Al-Majali Y, Wisner B, Mastorakos IN, Hunyadi Murph SE, Paramsothy M (eds) Advances in Sustainable Composites. TMS 2025. Springer, Cham. https://doi.org/10.1007/978-3-031-81057-2_17

Luo S, Ke J, Yuan M, Zhang Q, Xie P, Deng L, Wang S. 2018. $CuInS_2$ quantum dots embedded in Bi_2WO_6 nanoflowers for enhanced visible light photocatalytic removal of contaminants. Appl Catal B Environ, 221: 215–222. https://doi.org/10.1016/j.apcatb.2017.09.028

Maya-Johnson S, Gracia L, Longo E, Andres J, Leite ER. 2017. Synthesis of cuboctahedral CeO_2 nanoclusters and their assembly into cuboid nanoparticles by oriented attachment. ChemNanoMat, 3(4): 228–232. https://doi.org/10.1002/cnma.201700005

Muthamizh S, Suresh R, Giribabu K, Manigandan R, Praveen Kumar S, Munusamy S, Narayanan V. 2015. $MnWO_4$ nanocapsules: synthesis, characterization and its electrochemical sensing property. J Alloys Compd, 619: 601–609. https://doi.org/10.1016/j.jallcom.2014.09.049

Nagaraja K, Mallika B, Arunpandian M, Ravindran E, Tae Hwan O. 2025. Green synthesis of gold-decorated $BaTiO_3$-ZnO nanocomposites using Arabic gum polymer for efficient photocatalytic degradation of emerging textile dyes, antimicrobial, and toxicological evaluation. Int J Biol Macromol, 311: 143396. https://doi.org/10.1016/j.ijbiomac.2025.143396

Nezzari A, Medina S, Khane Y, Boublenza H, Guezzoul M, Zoukel A, Amrani B. 2025. Photocatalytic degradation of brilliant green dye using Cu_2NiSnS_4 thin films under ultraviolet irradiation. Inorg Chem Commun, 174: 114021. https://doi.org/10.1016/j.inoche.2025.114021

Nogami A, Suzuki T, Katsufuji T. 2008. Second harmonic generation from multiferroic $MnWO_4$. J Phys Soc Jpn, 77(11): 115001. https://doi.org/10.1143/JPSJ.77.115001

Pirhashemi M, Habibi-Yangjeh A. 2018. Fabrication of novel ZnO/$MnWO_4$ nanocomposites with p-n heterojunction: visible-light-induced photocatalysts with substantially improved activity and durability. J Mater Sci Technol, 34(10): 1891–1901. https://doi.org/10.1016/j.jmst.2018.01.014

Rao A, Cölfen H. 2017. Facet control in nanocrystal growth. In: Atwood JL (Ed.), Comprehensive Supramolecular Chemistry II. Elsevier, UK, London, pp: 129–156. https://doi.org/10.1016/B978-0-12-409547-2.12638-1

Rastin H, Dell'Angelo D, Sayede A, Badawi M, Habibzadeh S. 2025. Green and sustainable metal-organic frameworks (MOFs) in wastewater treatment: a review. Environ Res, 282: 122087. https://doi.org/10.1016/j.envres.2025.122087

Sahoo S, Reddy GBT, Mahamallik P. 2024. Sunlight-assisted photocatalytic degradation of methyl red using g-C_3N_4 as metal-free photocatalyst. In: Mazumder D (ed.) Sustainable Advanced Technologies for Environmental Management. Springer Proc Earth Environ Sci. Springer, Cham, London, UK, pp: 62. https://doi.org/10.1007/978-3-031-64006-3_1

Shalini S, Sasikala T, Tharani D, Venkatesh R, Muthulingam S. 2024. Novel green CQDs/ZnO binary photocatalyst synthesis for efficient visible light irradiation of organic dye degradation. J Mol Liq, 410: 125525. https://doi.org/10.1016/j.molliq.2024.125525

Shamshad J, Ur Rehman R. 2025. Innovative approaches to sustainable wastewater treatment: a comprehensive exploration of conventional and emerging technologies. Environ Sci Adv, 4(2): 189–222. https://doi.org/10.1039/D4VA00136B

Shivaganga GS, Parameswara P, Mallikarjunaswamy C, Kumar KCS, Soundarya TL, Nagaraju G, Ranganatha VL. 2023. Green, nonchemical route for the synthesis of $MnWO_4$ nanostructures: photocatalytic and electrochemical performance. J Mater Sci Mater Electron, 34(25): 1791. https://doi.org/10.1007/s10854-023-11190-3

Siahsahlan M, Mohammadi Aref S, Naghshara H, Azmayesh R. 2025. The effects of reduced graphene oxide amount on the photocatalytic performance of TiO_2 nanoparticles for hydrogen evolution. Int J Hydrogen Energy, 142: 318–329. https://doi.org/10.1016/j.ijhydene.2025.05.411

Vosoughifar M. 2017. Preparation, characterization, and morphological control of $MnWO_4$ nanoparticles through novel method and its photocatalyst application. J Mater Sci Mater Electron, 28(2): 2135–2140. https://doi.org/10.1007/s10854-016-5777-6

Wang G, Xu J, Sun Z, Zheng S. 2020. Surface functionalization of montmorillonite with chitosan and the role of surface properties on its adsorptive performance: a comparative study on mycotoxins adsorption. Langmuir, 36(10): 2601–2611. https://doi.org/10.1021/acs.langmuir.9b03673

Wu W, Qin W, He Y, Wu Y, Wu T. 2012. The effect of pH value on the synthesis and photocatalytic performance of $MnWO_4$ nanostructure by hydrothermal method. J Exp Nanosci, 7(4): 390–398. https://doi.org/10.1080/17458080.2010.533293

Xue W, He H, Zhu J, Yuan P. 2007. FTIR investigation of CTAB–Al–montmorillonite complexes. Spectrochim Acta A Mol Biomol Spectrosc, 67(3): 1030–1036. https://doi.org/10.1016/j.saa.2006.09.024

Zargazi M, Entezari MH. 2019. Sonochemical versus hydrothermal synthesis of bismuth tungstate nanostructures: photocatalytic, sonocatalytic and sonophotocatalytic activities. Ultrason Sonochem, 51: 1–11. https://doi.org/10.1016/j.ultsonch.2018.10.010

Zhang D, Otitoju TA, Ouyang Y, Shoparwe NF, Wang S, Li S. 2021. A review on metal ions modified TiO_2 for photocatalytic degradation of organic pollutants. Catalysts, 11(9): 1039. https://doi.org/10.3390/catal11091039

Zheng M, Zhang H, Gong X, Xu R, Xiao Y, Dong H, Liu Y. 2013. A simple additive-free approach for the synthesis of uniform manganese monoxide nanorods with large specific surface area. Nanoscale Res Lett, 8(1): 166. https://doi.org/10.1186/1556-276X-8-166